



# Diesel soot mass calculation in real-time with a differential mobility spectrometer

Jonathan P.R. Symonds<sup>a,\*</sup>, Kingsley St.J. Reavell<sup>a</sup>, Jason S. Olfert<sup>b</sup>,  
Bruce W. Campbell<sup>a</sup>, Stuart J. Swift<sup>b</sup>

<sup>a</sup>*Cambustion Ltd., J6 The Paddocks, 347 Cherry Hinton Road, Cambridge CB1 8DH, UK*

<sup>b</sup>*Cambridge University Engineering Department, Trumpington Street, Cambridge, CB2 1PZ, UK*

Received 25 July 2006; received in revised form 2 October 2006; accepted 2 October 2006

---

## Abstract

This paper presents a methodology to allow a real-time particle size spectrometer to produce a mass concentration output by calculation from its electrical mobility response. As part of this, a Bayesian statistical algorithm for parametrising spectral data from the Cambustion DMS500 in terms of a number of lognormal functions is outlined, allowing the nucleation and accumulation modes of a Diesel aerosol to be treated separately and also to reduce mass calculation noise and improve spectral resolution. Previous literature is combined with new experimental results to develop a size:mass power-law relationship for this instrument. The effective density as a function of size for this instrument is found to be closer to that for water droplets than equivalent relationships for DMA/SMPS measurements in the literature, therefore making DMS500 mass calculation less susceptible to error from liquid adsorbed on agglomerates. The technique is validated with two Diesel engines against the gravimetric methods of filter paper and Diesel particulate filter (DPF) weighings. Good agreement is achieved over a variety of engine conditions, with the mean and standard deviation of the percentage difference of the calculated mass concentration from DPF weighings being  $-12.1 \pm 11.4\%$  and from filter paper weighings being  $-15.1 \pm 18.0\%$ . The calculated mass concentrations are systematically below those of the gravimetric methods.

© 2006 Elsevier Ltd. All rights reserved.

*Keywords:* Diesel; DMS; Particulate mass; Lognormal; Fractal

---

## 1. Introduction

### 1.1. Background

Particles are generated from a variety of sources, both natural and anthropogenic; and the emissions from internal combustion engines are one of the major global sources of particulate matter (PM). PM is known to contribute to climate change, reduce visibility, and affect human health. To reduce the environmental impact of internal combustion engines, governments regulate the mass of PM emitted by vehicles. Current particulate air quality regulations and diesel PM regulations from the US Environmental Protection Agency (EPA) and the EU are typically based on a gravimetric

---

\* Corresponding author. Tel.: +44 1223 210250; fax: +44 1223 210190.

E-mail address: [jps@cambustion.co.uk](mailto:jps@cambustion.co.uk) (J.P.R. Symonds).

filter method. However, it is well documented that gravimetric filter measurements can be affected by a variety of artefacts. These artefacts include adsorption of vapour onto the filter, volatilisation of semi-volatile compounds from filtered particles, and an array of chemical reactions between filtered particles, the gas, and filter substrate (Hinds, 1999; Patashnick, Rupprecht, Ambs, & Meyer, 2001; Zhang & McMurry, 1987). Another problem with gravimetric filter measurements is that long sampling times are required for adequate measurement resolution and as future emission standards tighten, gravimetric methods may not be feasible for such small amounts of accumulated mass. Also, due to the nature of filter measurements, transient mass concentration measurements cannot be made, making the task of reducing particulate emissions by engine calibration difficult.

Besides filter-based methods, various instruments and methods can be used to measure mass concentrations or mass distributions. Firstly, a tapered element oscillating microbalance (TEOM) can be used to measure real-time mass concentrations (Chan & He, 1999; Morawska, Johnson, Ristovski, & Agranovski, 1999; Saito & Shinozaki, 1990). However, like filter measurements, the TEOM is affected by sampling artefacts and cannot provide size-resolved data. Secondly, light scattering measurements can be used to estimate particle mass concentration (Sioutas, Kim, Chang, Terrell, & Gong, 2000; Thomas & Gebhart, 1994); however, the relationship between light scattering and particle mass is empirical and light scattering methods will not be accurate in transient measurements if the size-distribution or refractive index of the aerosol changes during a test. Thirdly, cascade impactors such the micro-orifice uniform deposit impactor (MOUDI; Marple, Rubow, & Behm, 1991) can be used to measure mass distributions by a gravimetric analysis of particle mass collected on each impactor substrate. However, this method is time consuming and the MOUDI suffers from the same sensitivity issues as filter measurements. Fourthly, acoustic resonance from laser heated soot can be used to measure mass (photoacoustic soot sensor, Petzold & Niessner, 1996). This method promises a direct mass measurement for most particle sizes but does not provide size information.

Particle sizing instruments can also be used to measure mass distributions if the particle density is known. Particle sizing instruments generally measure the aerodynamic equivalent diameter of particles, such as the electrical low pressure impactor (ELPI; Ahlvik, Ntziachristos, Keskinen, & Virtanen, 1998), the mobility equivalent diameter, such as the scanning mobility particle sizer (SMPS; Wang & Flagan, 1990), or the electrical mobility equivalent diameter (see Section 4.1 for a definition) such as the differential mobility spectrometer (DMS; Reavell & Hands, 2002), or engine exhaust particle sizer (EEPS; Johnson, Caldwell, Pocher, Mirme, & Kittelson, 2004). A hybrid inertial and electrical size classification instrument, the Dekati mass monitor (DMM) is also produced (Lehmann, Niemelä, & Mohr, 2004).

In early studies with ELPI and SMPS mass measurements, a uniform particle density was assumed. However, it was found that for fractal-like structures such as diesel particulates, assumptions of uniform particle density resulted in large uncertainties in mass measurement (Andrews, Clark, Rojas, Sale, & Gregory, 2001; Peters, Chein, & Lundgren, 1993; Sioutas, Abt, Wolfson, & Koutrakis, 1999). The uncertainty in this method can be greatly reduced by measuring or assuming a size-dependent particle density. The density of particles can be measured by using a differential mobility analyser (DMA) and an ELPI and using the relationship between mobility and aerodynamic equivalent diameters (see Eq. (11)), as shown by Maricq and Xu (2004). The size-dependent density of particles can also be found using a DMA and a centrifugal particle mass analyser, such as the APM (aerosol particle mass, Ehara, Hagwood, & Coakley, 1996) or Couette centrifugal particle mass analyser (CPMA) (Olfert & Collings, 2005), which measures the mass of particles. From these studies size-dependent density functions for diesel particles have been obtained which can be used to calculate the mass distribution and mass concentration of particles measured with mobility sizing instruments.

These functions are usually represented in form  $M \propto D^i$  for mass  $M$ , particle diameter  $D$ , and fitted index,  $i \in \mathbb{R}^+$ . When  $i = 3$  this expression reduces to the trivial case for spherical particles, when  $i \notin \mathbb{N}$  the expression represents a fractal structure (e.g. Mandelbrot, 1983). In this paper, a method is described which builds upon these principles to determine mass concentration in real-time from spectral data produced by the Combustion DMS500 real-time particle sizing instrument. As part of this method, a new software algorithm to parametrise spectral data in terms of multiple lognormal modes is also presented. Validation data from Diesel engines is given to compare with gravimetric methods.

## 1.2. Overview of method

The method of mass calculation used in this paper has three distinct parts: (1) the particle spectrometer and sampling system, (2) the novel lognormal fitting software, and (3) the derivation of a specific mass weighting expression

for this instrument. The instrumentation is described in Section 2.1. The use of a lognormal fit to constrain spectral aerosol data has several advantages in terms of a mass calculation scheme if the data are suspected to be lognormal in form. Firstly, to calculate mass from a binned spectrum, an expression of the form  $\rho \sum_D D^i$ , where  $i \sim 3$ , is used. This means that the mass is very sensitive to large  $D$  and hence noise at the upper size end of a spectrum can become amplified to a great extent. The use of a lognormal function suppresses any noise in the tail of the spectrum. Secondly, a diesel engine spectrum can consist of at least two separate modes, with a nucleation mode (consisting of volatile organic fraction (VOF), sulphate or water) present in the sub 30 nm range under certain engine and dilution conditions. This mode may partially overlap the accumulation mode, and thus it is useful to be able to separate and individually weight the two compositionally different components to calculate overall mass. Fitting a separate lognormal function to each accomplishes this, whilst still allowing mode overlap, something not possible with a simple size based spectral cut-off. Thirdly, it reduces the volume of data from the instrument; the size spectrum is described by only the count median diameter (CMD), geometric standard deviation (GSD or  $\sigma_g$ ) and number concentration for each mode. This allows direct mass calculation by using the Hatch–Choate relationship for the diameter of average mass,  $D_{\bar{m}} = \text{CMD} \exp(\frac{i}{2} \ln^2(\sigma_g))$  (e.g. Hinds, 1999), and then weighting this directly by the index,  $i$ . The lognormal data processing algorithm also has advantages in terms of spectral resolution (see Section 3.2).

The algorithm used does not fit lognormal functions directly to the processed DMS size spectrum; it returns the lognormal functions which best represent the instrument's raw response to the aerosol, given its calibrated transfer function. An offline, non-automated bimodal lognormal fit to the instrument's response to an aerosol was first used to process mass calculation data by Kittelson et al. (2004). Section 3 describes the new algorithm and quantifies its effectiveness at the above objectives.

The data in Kittelson et al. (2004) show that DMS mass calculation was more accurate with a weighting index of 3 than with the fractal dimensions of  $2 < i < 3$  previously suggested for DMA classification (e.g. Park, Cao, Kittelson, & McMurry, 2003). Section 4.2 offers an explanation for this based upon differences in agglomerate charging between bipolar and unipolar charging spectrometers, and a more precise mass weighting rule for the DMS500 is calculated.

Experimental validation is in terms of both weighed filter papers, with diluted exhaust from a constant volume sampler (CVS) tunnel, and by weighing the engines' loaded Diesel particulate filter (DPF) whilst hot.

The block diagram in Fig. 1 may help to illustrate the overall scheme.

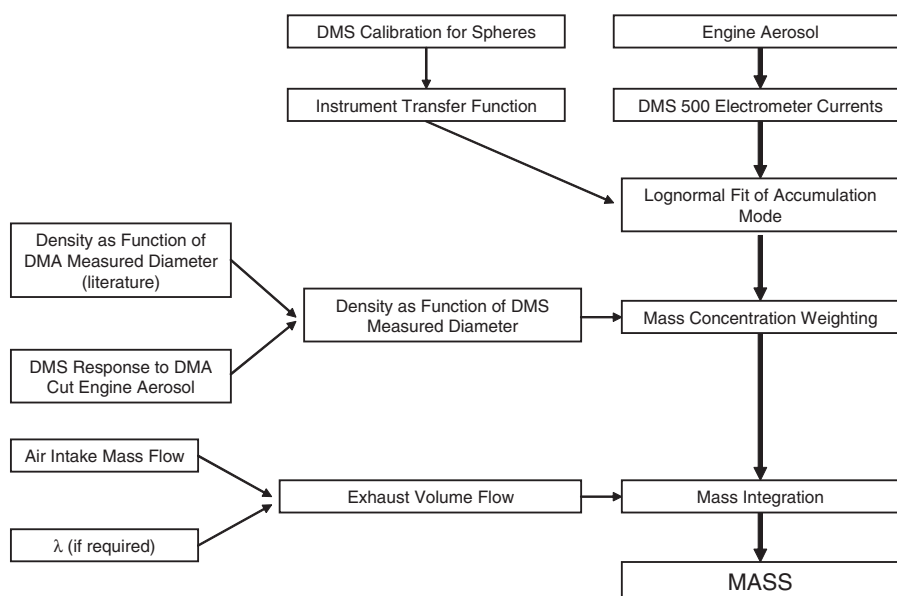


Fig. 1. Block diagram of mass calculation method.

## 2. Equipment

### 2.1. Instrumentation

The DMS500 (Reavell, 2002; Reavell & Hands, 2002) was the first commercially available real-time differential mobility particle spectrometer. This was followed by the TSI EEPS (Johnson et al., 2004), TSI fast mobility particle sizer (FMPS) and Cambustion DMS50. All of these instruments use variations on the basic principle developed by Tartu University, Estonia from the 1980s onwards (Mirme et al., 1984) as the electrical aerosol spectrometer (EAS). They all consist of a corona diffusion charger mounted on a classification column consisting of a central rod held at high voltage and a series of collection rings connected to sensitive electrometers along the length of the column, co-axial to the rod. Charged particles enter the classification column and are carried towards the bottom by a flow of sheath air. Particles are deflected by the electric field from the central rod towards the collection rings; particles with a greater charge: aerodynamic drag ratio are collected nearer the top of the column. The charged particles produce signals on the electrometers, and these signals are processed to produce a real-time size versus concentration spectrum. A schematic of the DMS500 is shown in Fig. 2.

The instrument operates at sub-atmospheric pressure (250 mb) to increase the possible size range to 5 nm–1  $\mu\text{m}$  (by moving the point in size space of mobility inversion, Biskos, Reavell, & Collings, 2005), improve the time response, reduce particle agglomeration and ensure less sensitivity to engine exhaust pressure fluctuations. The instrument has a built-in 2-stage dilution, and a heated line for direct exhaust sampling, as used in this paper (Fig. 3). The first stage consists of up to 4:1 dilution with metered, HEPA filtered, pre-warmed air close to the sampling point. This is mainly to prevent condensation of water vapour in the instrument. The diluted aerosol is then dropped to 250 mbar through a critical orifice which gives a concentration reduction equivalent to primary dilution of 16:1. The use of a critical orifice is also common in engine aerosol sampling in conjunction with an ejector diluter (e.g. Khalek, Kittelson, & Brear, 2000; Kittelson, Watts, & Johnson, 2002) with no notable adverse effect upon agglomerates. For the ca. 1 mm orifice hole in use here, calculations based upon the work of Pich (1964) show negligible impaction losses over the size range of this instrument. Also, a study using a critical orifice and ejector pump to mimic the DMS500 orifice, internal pressure and aerosol residence time shows negligible effects upon volatile aerosols (Symonds, Collings, Reavell, & Kittelson, 2004).

The aerosol then passes through 5 m of silicone tubing heated (in this work) to 55  $^{\circ}\text{C}$ . This line length decreases the time response to around 300 ms. Once in the instrument, the aerosol is further diluted with an integral mechanical rotating disc diluter, custom designed for the DMS series. The main 8 slpm of flow passes straight through one of several holes in a disc, is HEPA filtered and then passes through a hole at 180 $^{\circ}$  to the first in the opposite direction. When the disc rotates, small pockets of aerosol are carried from the dirty stream into the cleaned stream. The spectrum is corrected in real-time for primary dilution based upon the flow of clean dilution air and the flow of the main air flow

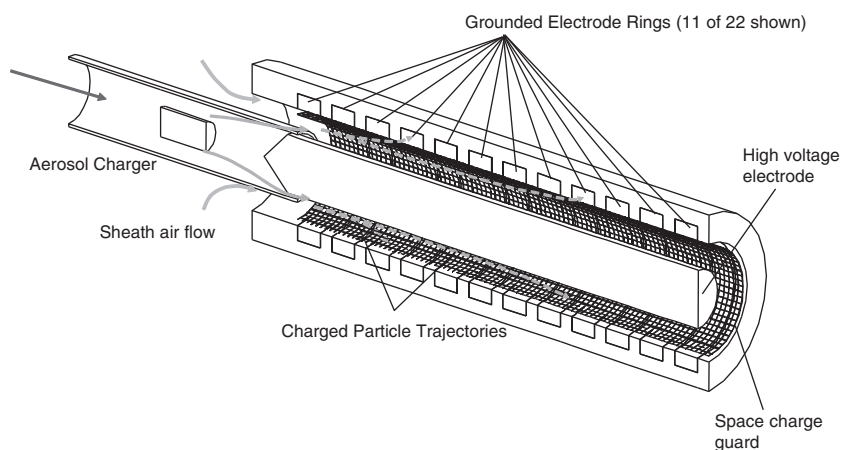


Fig. 2. Schematic of DMS500.

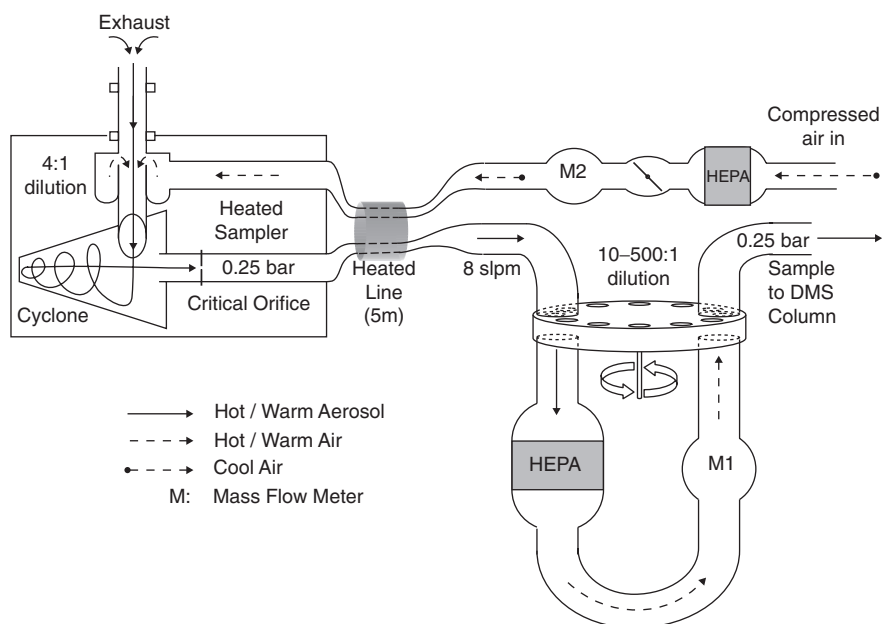


Fig. 3. Sampling system.

through the secondary diluter after HEPA filtration. Correction for the secondary diluter is made from the feed-back motor speed.

Data processing occurs on the desktop computer controlling the instrument. The raw signals from the 22 electrometers are processed to give a 38 channel spectrum by numerical solution by constraining the resultant spectrum to be continuous, smooth and always positive in concentration (see Section 3.1). The instrument is initially calibrated based upon a numerical model of the charging process and a Monte Carlo simulation (Reavell, 2002) of the particle trajectories in the column. The size calibration is then adjusted as necessary to agree with NIST traceable polystyrene latex (PSL) spheres ( $50 \text{ nm} \leq D \leq 900 \text{ nm}$ ) and by comparison with an SMPS system ( $5 \text{ nm} < D < 50 \text{ nm}$ ) with re-nucleated sulphuric acid (Symonds et al., 2004) and sodium chloride. Gain is set with reference to a known current source and a traceable mass flow meter.

## 2.2. Test engines

Two engines were used, representative of modern light duty diesel systems. To maximise the range of validation, one was in a vehicle on chassis rolls, sampling using a CVS tunnel (and to facilitate future on-road validation with the Cambusion DMS50 mobile particle sizer) and the other on an engine dynamometer, sampling using the built-in secondary diluter. The fuel systems were from different manufacturers for contrast.

Engine 'A' was a 2.2l common rail, 4-cylinder diesel engine on a UK 2002 specification Peugeot 406 with a 5-speed manual transmission and ca.  $10^5 \text{ km}$  of pre-usage. The emissions after-treatment system consists of a Diesel oxidation catalyst (DOC) directly upstream of a DPF within the same enclosure. The DOC was removed before the DPF based mass calculation tests detailed herein to minimise  $\text{NO} \rightarrow \text{NO}_2$  oxidation, as  $\text{NO}_2$  can in turn oxidise carbon in the DPF (known as passive regeneration). UK market low-sulphur diesel was used for the experiments, legislated to below 50 ppm sulphur. The vehicle was mounted on a 48" diameter, single roller chassis dynamometer and was driven by a robot driver, both manufactured by Froude Hofmann Ltd. The experimental set-up (as well as post-DPF particulate and pre/post-DPF gas analysis from this vehicle) is described by (Campbell, Peckham, Symonds, Parkinson, & Finch, 2006).

Engine 'B' was a 2.0l, high pressure common rail, variable-geometry turbocharged Diesel engine with intercooler and exhaust gas recirculation (EGR) cooler. It was fitted with a DOC and was connected to an engine dynamometer

(Alstom Alspa PGD4282-4002 unit driving a Sicmemotori ACVA180MB 125 kW (382 Nm) three-phase motor). This engine was run under an experimental engine control system.

### 3. Real-time lognormal fit to instrument kernel

#### 3.1. Algorithm development

The (non-lognormal) spectrum vector,  $\mathbf{s}$ , from the measured DMS500 electrometer ring current vector,  $\mathbf{i}$ , is obtained by minimising the error term,  $\mathbf{e}$  in the following relationship:

$$\mathbf{i} = \mathbf{A}\mathbf{s} + \mathbf{e}, \quad (1)$$

where  $\mathbf{A}$  is a matrix representing the instrument transfer function. This is achieved by least squares minimisation with linear regularisation and a non-negative constraint.

Replacing the spectrum with a lognormal function,  $\mathbf{l}(\mu, \sigma_g)$ :

$$\mathbf{i} = n\mathbf{A}\mathbf{l}(\mu, \sigma_g) + \mathbf{e}, \quad (2)$$

where  $\mu$  is CMD,  $\sigma_g$  is GSD and  $n$  is the particle number concentration in the mode. A solution for  $\mu$ ,  $\sigma_g$  and  $n$  can be found by minimising  $\mathbf{e}$ . For a multi-lognormal fit, Eq. (2) becomes

$$\mathbf{i} = n_1\mathbf{A}_1\mathbf{l}(\mu_1, \sigma_{g1}) + n_2\mathbf{A}_2\mathbf{l}(\mu_2, \sigma_{g2}) + \dots + n_m\mathbf{A}_m\mathbf{l}(\mu_m, \sigma_{gm}) + \mathbf{e}. \quad (3)$$

Note that this also allows the use of different instrument transfer functions for separate aerosol components, so for example, differing aerosol charging models or calibrations (e.g. for differing equivalent diameters, mobility, aerodynamic etc.) can be applied to agglomerates than to nucleation material.

In practice, this optimisation is performed by maximising the *posterior probability* of the lognormal parameters within a Bayesian statistical framework. Bayes' theorem (e.g. Sivia, 1994) states for a set of data  $D$  described by parameters  $\mathbf{w}$

$$P(\mathbf{w}|D) = \frac{P(\mathbf{w})P(D|\mathbf{w})}{P(D)}. \quad (4)$$

In this case  $\mathbf{w}$  are the lognormal parameters  $n_m$ ,  $\mu_m$  and  $\sigma_{gm}$  and the data are the measured electrometer currents  $\mathbf{i}$ .  $P(\mathbf{w}|D)$  is the posterior probability to be maximised.  $P(D|\mathbf{w})$  is known as the *likelihood* and represents the probability of the measured electrometer currents given a set of parameters.  $P(D)$  is a normalisation constant that can be ignored.

A set of electrometer currents  $\mathbf{j}$  can be obtained from a set of parameters  $\mathbf{w}$  by means of

$$\mathbf{j}(\mathbf{w}) = \mathbf{A}\mathbf{s}(\mathbf{w}). \quad (5)$$

For each electrometer, the probability of the measured electrometer current,  $i$ , given the guessed electrometer current  $j$  (and hence the parameters) are correct, is assumed to be normally distributed with a standard deviation equal to the instrumental noise on that electrometer,  $\sigma$ :

$$P(i|j, \sigma) = \frac{1}{\sigma\sqrt{2\pi}} \exp\left(-\frac{(i-j)^2}{2\sigma^2}\right). \quad (6)$$

As the noise on each electrometer can be assumed to be independent, the total likelihood is given as

$$P(D|\mathbf{w}) = \prod_{k=1}^{22} \frac{1}{\sigma_k\sqrt{2\pi}} \exp\left(-\frac{[i_k - j_k(\mathbf{w})]^2}{2\sigma_k^2}\right). \quad (7)$$

The instrument has an electrometer zero offset subtraction feature, during which the rotating disc diluter in Fig. 3 is stopped so that all the air flow into the classifier is HEPA filtered. During this process, the true instrument noise base is measured so it can be applied to the fit as in Eq. (7) and is also displayed on the user interface.

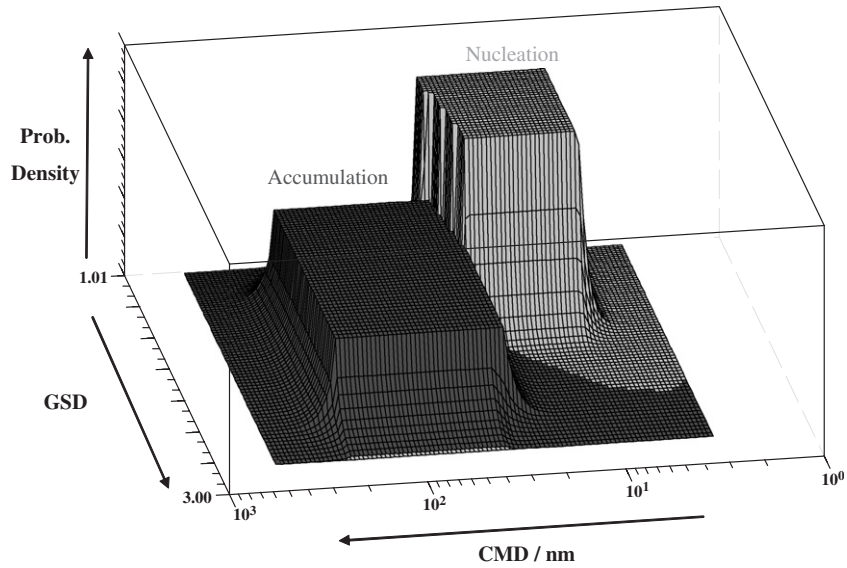


Fig. 4. Example prior probability map for Diesel aerosol.

The term  $P(\mathbf{w})$  in Eq. (4) is known as the *prior probability*. It represents the a priori knowledge about a system before the data is examined. In this case, it can be used to loosely bind the particulate modes to be within a range of sizes and GSDs by specifying the probability in regions of  $(\mu, \sigma_g)$  space. For Diesel combustion aerosol, this is used to constrain and separate the nucleation and accumulation modes. Fig. 4 shows an example probability map for Diesel combustion aerosol. Such a map is contained within a configuration file specific to a type of aerosol and a particular instrument's calibration.

It is also important that the true number of modes actually present is returned; when a mode is not present in significance above the noise base of the instrument then an amplitude of 0.0 is returned. Again, Bayes' theorem is used as a *model selector* to determine the most probable combination of modes present. Let  $P(\mathcal{H}_m|D)$  be the probability of there truly being  $m$  modes present given the data (measured electrometer currents). Then by Bayes' theorem

$$P(\mathcal{H}_m|D) = \frac{P(\mathcal{H}_m)P(D|\mathcal{H}_m)}{P(D)}. \quad (8)$$

No particular number of modes is favoured a priori so we assume  $P(\mathcal{H}_m)$  is uniform. Using the identity  $P(X|I) \equiv \int_{-\infty}^{+\infty} P(X, Y|I) dY$  (known as *marginalisation*),

$$P(D|\mathcal{H}_m) = \int \dots \int P(D, \mathbf{w}|\mathcal{H}_m) d^m \mathbf{w}, \quad (9)$$

is obtained. The identity  $P(Y, X|I) \equiv P(Y|X, I)P(X|I)$  (the *product rule*) can be used to rewrite the integrand of Eq. (9) in terms of known quantities as

$$P(D, \mathbf{w}|\mathcal{H}_m) = P(D|\mathbf{w}, \mathcal{H}_m)P(\mathbf{w}|\mathcal{H}_m), \quad (10)$$

where the terms on the right are the same as those in the numerator of Eq. (4) but now specific to a certain combination of modes. The evaluation of Eqs. (8)–(10) in real time (10 Hz) on a desktop PC running the DMS500 presented a considerable challenge in code optimisation.

### 3.2. Testing

The effect on measurement noise, both in terms of total number and total mass, was investigated by generating a instrument response (electrometer currents,  $\mathbf{i}$ ) from a series of pure lognormal functions,  $n\mathbf{l}(\mu, \sigma_g)$ , added to noise

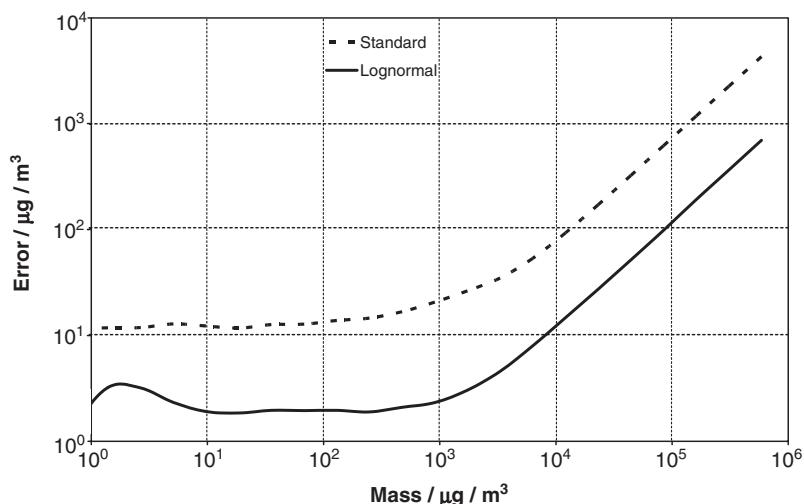


Fig. 5. Mass noise floor of DMS500 for 60 nm,  $\sigma_g = 1.9$  aerosols of varying amplitude.

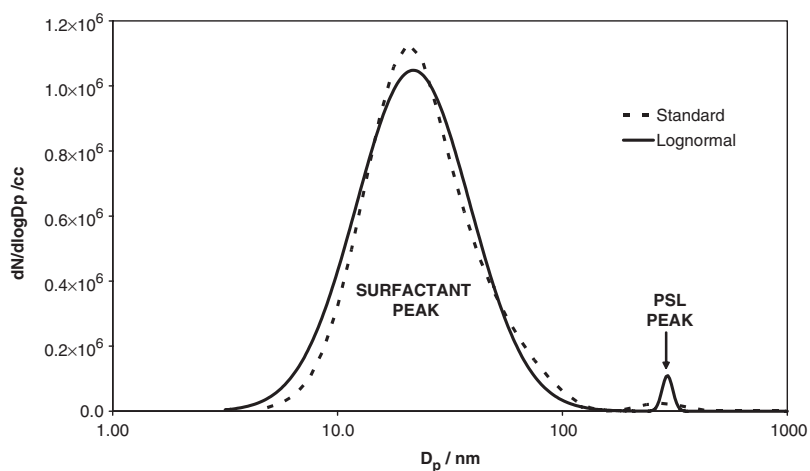


Fig. 6. 299 nm PSL spheres measured with the DMS500 with both reconstructed lognormal and full spectral outputs.

(e) measured from a DMS500 as in Eq. (2). In this case ( $\mu = 60$  nm,  $\sigma_g = 1.9$ )  $n$  was steadily attenuated over the data set such that  $10^7 \geq n(\text{N cm}^{-3}) \geq 1$ . The lognormal parameters were recovered with the Bayesian algorithm, and the standard deviation of total mass calculated from the recovered parameters, based upon the weighting described in Section 4.2, was plotted versus true mass. The results are shown in Fig. 5 compared with those from the non-lognormal data processing algorithm (in the latter case bin-wise weighted and then summed). The local maximum towards low  $M$  is an artefact of the algorithm increasingly ignoring modes altogether as the noise base is reached. An improvement of up to nine times in mass sensitivity is observed, giving a mass sensitivity of 0.1% of reading  $+2 \mu\text{g m}^{-3}$ .

The lognormal constraint also has the effect of improving the resolution of the instrument (for intrinsically lognormal aerosols), in terms of minimum  $\sigma_g$  measurable without broadening. Fig. 6 shows an aerosol consisting of a nebulised aqueous suspension of 299 nm PSL spheres (Duke Scientific 3000 series), which have been dried in a diffusion dryer and radioactively neutralised. It was measured with a DMS500 using both regular and lognormal data processing (a different set of priors is used for PSL and Diesel aerosols). The lognormal algorithm returns a GSD of 1.07, compared with 1.23 for the regular spectrum. The PSL size distribution is specified as having a standard deviation of 4.1 nm

which gives an approximate ideal GSD  $\simeq (299 + 4.1)/299 = 1.014$ , given that the distribution is very narrow. Note that whilst both the width and height of the PSL mode with the differing methods are quite different, the total number concentrations ( $\sim$  area under the spectrum) are within 12% of each other. The difference in mass (assuming unit density and an index of 3) is 11%.

In principle, there is no limit to the number of modes which can be fitted, if appropriate priors are used; in practice current available desktop computing power limits this to two modes for real-time operation. However, post-processing of trimodal (non-engine) data has been successfully demonstrated. Automatic discrimination of multiple modes in different applications may require characterisation of the typical aerosol parameters. For non-lognormal modes the CMD of the lognormal function may not coincide with the peak of the discrete spectrum but is still very close to the latter's calculated CMD. However, even for skewed spectra, the total number and mass are in close agreement with those calculated from the discrete spectrum.

## 4. Spectral weighting to calculate mass

### 4.1. Previous work

There have been several studies investigating the effective density of diesel aerosol agglomerates. The following definitions of diameter are often used (Kasper, 1982):  $D_{ae}$ —aerodynamic equivalent diameter, the size determined by inertial means;  $D_{me}$ —mechanical mobility equivalent diameter, as sized by mobility spectrometers such as the SMPS. The concept of  $D_{me}$  is further complicated by the complex charging properties of agglomerates. This is especially true for instruments which multiply charge using a corona discharge (such as the DMS500, EEPS, FMPS and DMS50). These instruments effectively classify by charge to drag ratio, or by electrical mobility. So it is helpful here to introduce another definition of diameter, that of electrical mobility equivalent diameter or  $D_{eme}$ . This is the diameter of a spherical particle with the same charge:drag ratio as the particle being measured. Whilst instruments which use bipolar charging (such as the DMA) also classify by electrical mobility, the few charges applied by this in the nanoparticle regime are generally well modelled and are easily deconvoluted due to the relatively large difference in electrical mobility going from  $1^+ \rightarrow 2^+ \rightarrow 3^+$  charges. Therefore, the DMA effectively gives pure mechanical mobility in the size range of Diesel nanoparticles. For spherical particles, on which the DMS500 calibration is based,  $D_{eme} = D_{me}$ .

Much work has been done to establish relationships between mobility and aerodynamic equivalent diameters, using the following relationship (Kasper, 1982; Park et al., 2003)

$$\rho_{\text{eff}} D_{\text{me}}^2 C_{\text{me}} = \frac{6m}{\pi D_{\text{me}}} C_{\text{me}} = \rho_0 D_{\text{ae}}^2 C_{\text{ae}}, \quad (11)$$

where  $\rho_{\text{eff}}$  is an effective density,  $\rho_0$  is unit density ( $1000 \text{ kg m}^{-3}$ ),  $m$  is particle mass and  $C$  are the appropriate Cunningham slip correction factors. As introduced in Section 1.1, variations on a method developed by Kelly and McMurry (1992) have been used by various authors (Ahlvik et al., 1998; Gulijk, Marijnissen, Makkee, Moulijn, & Schmidt-Ott, 2004; Maricq & Xu, 2004) using DMA selected aerosol measured with an ELPI to determine this effective density. McMurry, Wang, Park, and Ehara (2002) developed a technique in which mobility classified aerosol selected by a DMA was directly mass measured by an APM. The APM consists of two co-axial cylindrical electrodes rotating at the same speed with a potential difference across them. Particles enter the gap between the electrodes and only exit if the opposed and competing centrifugal and electrical forces acting upon them are balanced. A CPC is then used to count those particles which make it through the mass band-pass. The electrode speed and potential difference can be scanned to build up a mass spectrum. Park et al. (2003) used this technique to determine effective densities for diesel agglomerates from light duty and heavy duty engines. The heavy duty engine data were taken at three different loads: 10%, 50% and 75%. If these data are plotted as mass (kg) versus  $D_{me}$  (DMA size/nm) then the following relationship is obtained from a power law fit:

$$M = 6.05 \times 10^{-24} \cdot D_{\text{me}}^{2.34}. \quad (12)$$

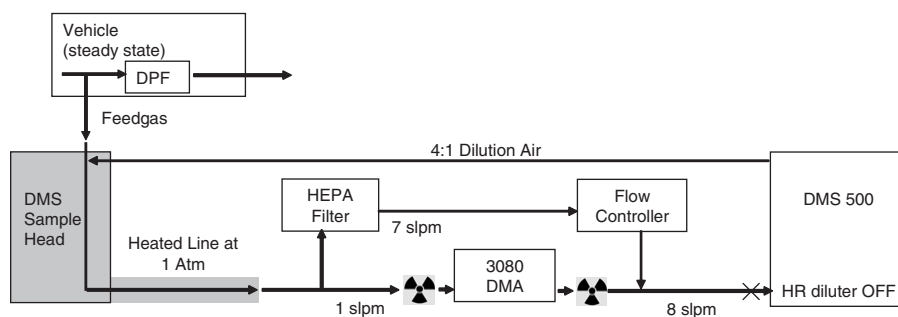


Fig. 7. Experiment to DMA select Diesel exhaust before sizing with the DMS500.

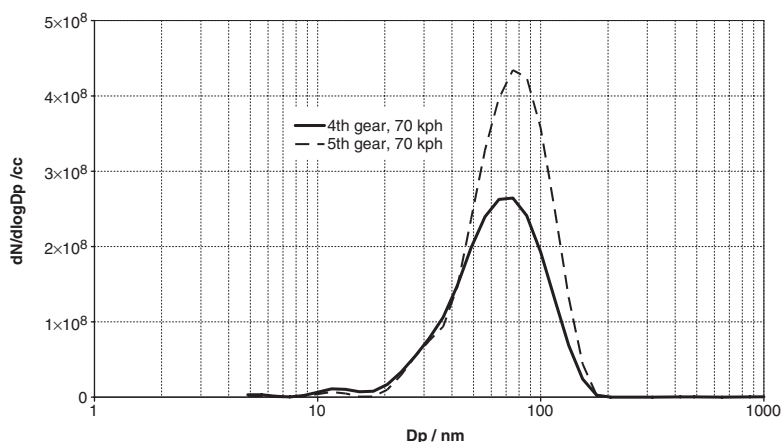


Fig. 8. Raw DMS500 spectra of steady-state test points for DMA selected experiment (averaged over 15 s, regular data processing algorithm).

A similar result was found by Olfert, Symonds, and Collings (2006) using a Couette CMPA on the light duty engine ‘A’ described in this work.

#### 4.2. A mass weighting for the DMS500

Firstly, a comparison between the drag based (mobility) agglomerate sizing of an SMPS and the charge:drag based (electrical mobility) agglomerate sizing of a DMS500 (calibrated for spheres) was made. The experimental set up used in Fig. 7 was used. A TSI 3080 DMA (3081 column) was inserted into the usual DMS500 sampling system, between the heated sample head and the instrument itself. The critical orifice was removed from the sample line and placed just prior to the instrument so that the DMA operated at atmospheric pressure. The 1 slpm of the 8 slpm required by the DMS passed through the DMA for size selection, and the other 7 slpm passed through a HEPA filter and a mass flow controller.  $^{85}\text{Kr}$  neutralisers were used either side of the DMA to (a) produce an equilibrium charge distribution for the DMA and (b) to re-equilibrate the charge post-DMA before sampling with the DMS. 4:1 primary dilution was used, and the rotating disc diluter in the DMS was in bypass mode. To give variation in the size of particles used, the vehicle of engine ‘A’ was run at two steady-state cruise conditions, taken from the New European Drive Cycle (NEDC) (a) 70 kph in 4th gear (15% load, 2000 rpm) and (b) 70 kph in 5th (top) gear (15% load, 1500 rpm). The particle size spectrum measured with the DMS (without DMA) for each of these conditions is shown in Fig. 8. The lognormal fitting software processed the DMA selected DMS data and Fig. 9 shows the comparison between  $D_{me}$  (DMA) and  $D_{eme}$  (DMS) for the diesel agglomerates. Little difference is observed between the two steady-state conditions.

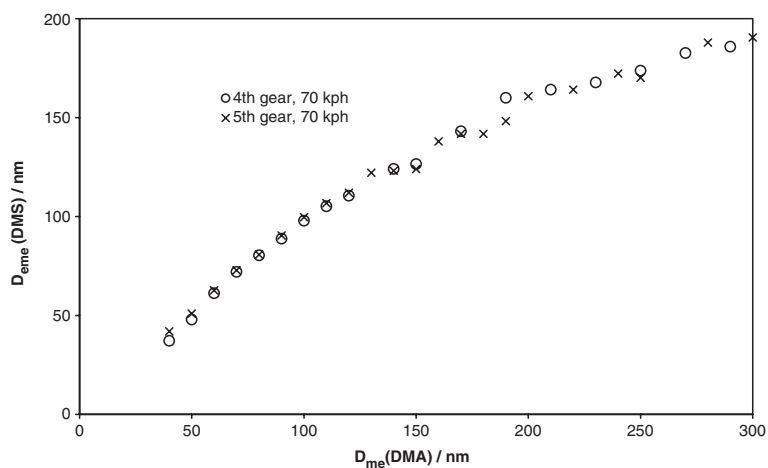


Fig. 9. Sphere-calibrated electrical mobility (DMS) sizing of mobility (DMA) selected Diesel engine agglomerates.

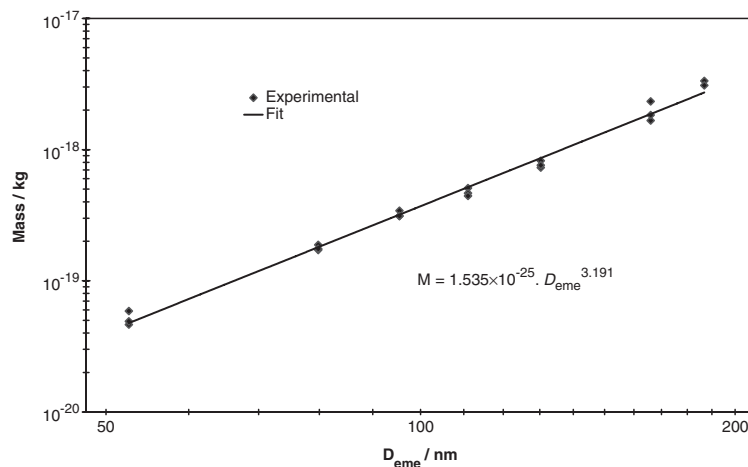


Fig. 10. APM selected aerosol measured with DMA data from Park et al. (2003) reprocessed with DMA:DMS agglomerate size relationship to give a mass: size rule for DMS500.

A quadratic fit to these data was then used to re-plot the Park et al. (2003) data in terms of  $D_{eme}$  versus mass, and a power law fit applied to this (Fig. 10), giving:

$$M = 1.54 \times 10^{-16} \cdot D_{eme}^{3.19}, \quad (13)$$

for size in nm and mass in  $\mu\text{g}$ . This relationship has been used for the validation tests in Section 5.

Fig. 11 shows the effective density of particles as a function of diameter, as defined in Eq. (11) but for  $D_{eme}$ , using Eq. (13). It has been shown that (for example) aftertreatment systems can change the effective density of soot by the adsorption of volatiles (e.g. Olfert et al., 2006). This might then cause concern that mass calculation from size spectral data would be very vulnerable to these effects. However, this plot shows that for size measurements by a DMS type instrument, the effective density of particles in the size range of interest (e.g. diameter of average mass = 130 nm for 85 nm,  $\sigma_g = 1.7$ ) is closer to the size independent  $1000 \text{ kg m}^{-3}$  limiting case for the adsorption of water when compared to DMA effective density data (as reported by Park et al., 2003) and thus the uncertainty due to unknown volatile fraction is likely to be smaller, but not non-existent. The validation data taken on engine 'B' (Section 5.3), which are

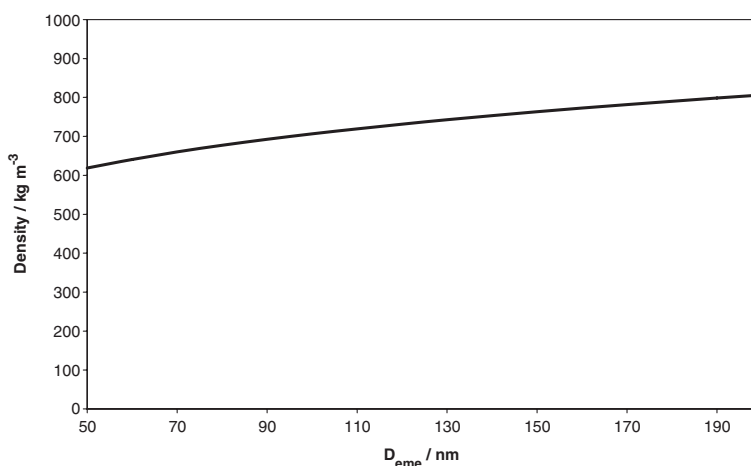


Fig. 11. Effective density of Diesel engine agglomerates for DMS sized aerosol, based upon power-law in Eq. (13).

completely independent of the data used to obtain the relationship in Eq. (13), will later give some confidence in the transferability of the relationship to other engines.

## 5. Experimental validation

In turn, each of the three experimental sections are now outlined: engine ‘A’ with DPF weighing, engine ‘A’ with filter paper in CVS tunnel and engine ‘B’ with DPF weighing. Then in Section 5.4 the validation results are pooled.

### 5.1. Diesel particulate filter weighings—engine ‘A’

Fig. 12 shows the experimental scheme. The standard DMS sampling system (Fig. 3) was connected to the engine exhaust (‘feedgas’). To calculate absolute mass (rather than mass concentration), the exhaust volumetric flow is required. Real-time exhaust flow has been used here as a weighting factor to obtain accurate average DMS mass concentrations over a test.

An engine air *intake* mass flow signal was taken from the engine electronic control unit (ECU) and fed to one of the DMS’s analogue inputs for logging alongside the spectral/mass data. This signal was pre-calibrated to *exhaust* mass (i.e. air and burnt fuel) flow using the CVS tunnel and  $\text{CO}_2$  tracing. The engine air intake flow meter has a faster time response than using  $\text{CO}_2$  tracing and thus is better for transient tests. All DMS measurements are referenced to S.T.P., so all volumetric flows are corrected to S.T.P. The DMS can perform these calculations internally to give a direct soot loading rate signal if a voltage to air flow calibration function is provided to the instrument user interface.

The relative air: fuel ratio,  $\lambda \equiv [\text{air} : \text{fuel}]_{\text{actual}} / [\text{air} : \text{fuel}]_{\text{stoichiometry}}$ , was also logged to the DMS via a Universal Exhaust Gas Oxygen (UEGO) sensor fitted to the vehicle’s tailpipe. For this vehicle, over an NEDC cycle,  $\langle \lambda \rangle \sim 2.3$ , with  $\lambda_{\text{min}} \sim 1.5$ . Over this range, the air intake signal to exhaust mass flow calibration will not vary more than a few percent as a result of changing fuelling conditions.

Thirdly, the vehicle road speed from the dynamometer was logged to a DMS analogue input. This allows other dynamometer and test cell data to be time-aligned with DMS data.

It would be somewhat facile to claim a mass correlation for a spectral instrument by just varying the particle concentration, so NEDCs were run to determine test points which would give a variety of particle sizes as well as concentrations. Fig. 13 shows the size of particles in the nucleation and accumulation modes over a typical NEDC as outputted by the software in lognormal mode. Of interest is also the particle number in each mode, Fig. 14 presents this during one acceleration–deceleration phase of the NEDC. Note how during acceleration and deceleration, the nucleation mode replaces the accumulation mode. On the acceleration, gear changes are clearly resolvable.

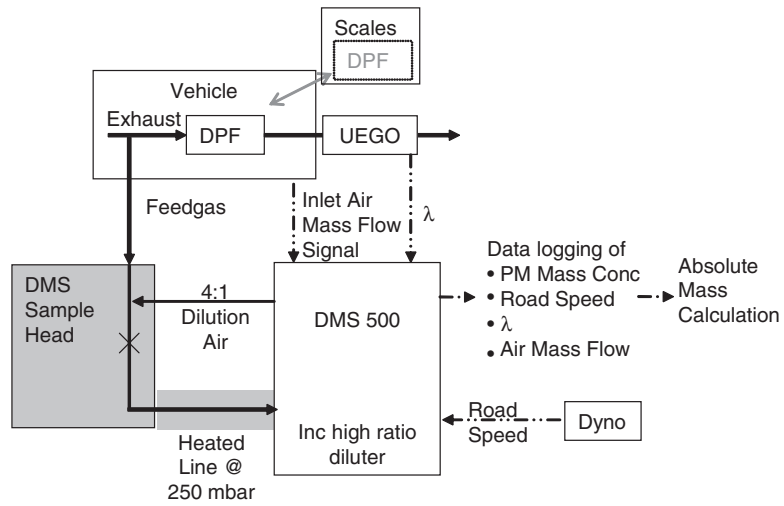


Fig. 12. Experiment to load DPF whilst monitoring feedgas with DMS500.

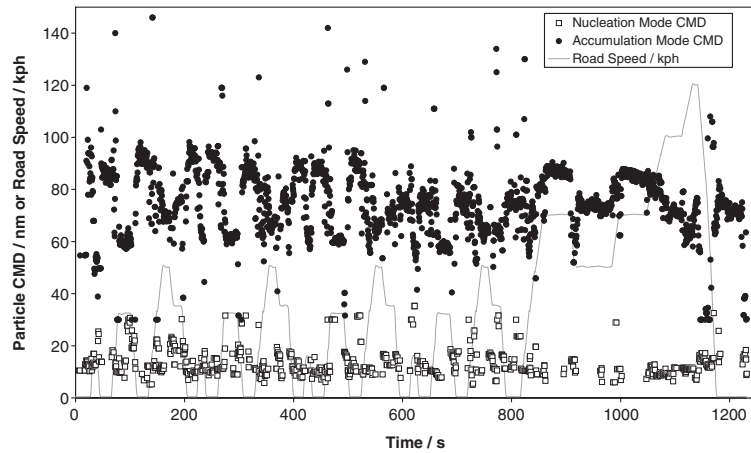


Fig. 13. Particle sizes over typical NEDC.

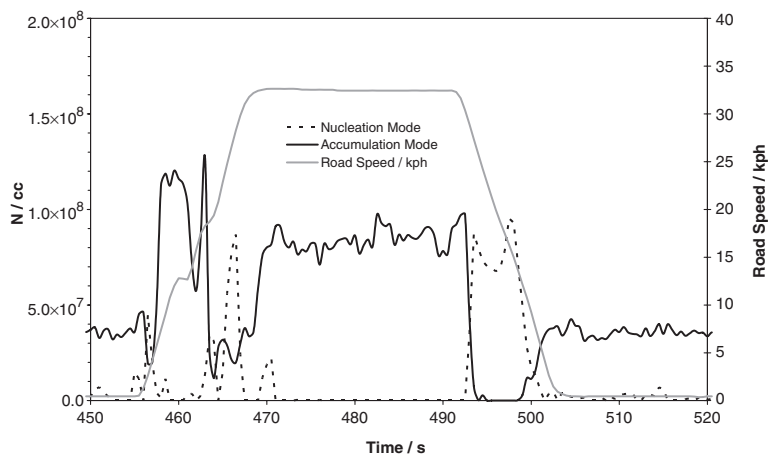


Fig. 14. Particle number over example section of NEDC.

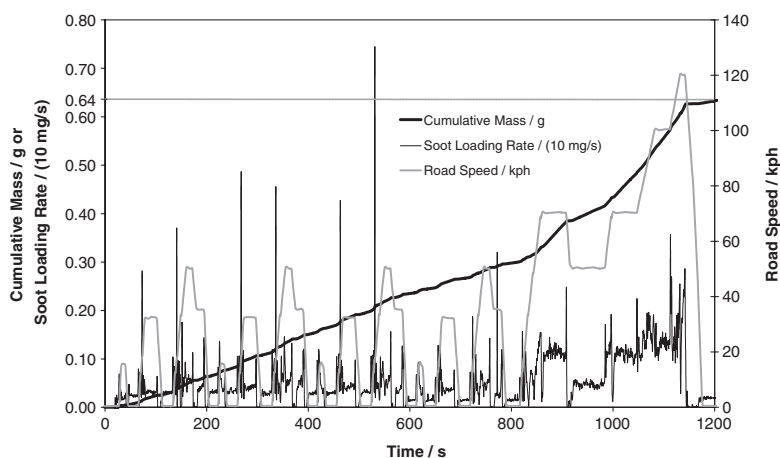


Fig. 15. DPF soot loading over NEDC.

Table 1

Results from DPF weighings on engine 'A'. EUDC is the Extra-Urban phase of the NEDC, i.e. post 800 s

Condition	Mean mass concentration/ $\mu\text{g cc}^{-1}$	
	DPF	DMS
6 NEDCs, 22 EUDCs, 3 Cruises	$3.49 \times 10^{-2}$	$3.22 \times 10^{-2}$
15% load, 2000 rpm	$3.41 \times 10^{-2}$	$3.06 \times 10^{-2}$
15% load, 1500 rpm	$5.82 \times 10^{-2}$	$6.77 \times 10^{-2}$
8% load, 2000 rpm	$2.19 \times 10^{-2}$	$2.05 \times 10^{-2}$

Fig. 15 shows the DMS calculated soot (i.e. accumulation mode) loading rate, using the weighting in Eq. (13) corrected for exhaust volumetric flow, as well as the cumulative soot mass over the cycle. The spikes in the soot rate are not due to time alignment errors, and are often due to a very rapid transient increase in particle size (see Fig. 13).

The DPF was weighed at elevated temperature ( $> 200\text{ }^{\circ}\text{C}$ ) after each test to avoid condensation of volatile material adding mass. The scale used had a resolution of 0.5 g, and the mass of soot collected was around 13 g on average. A summary of the test conditions and results is shown in Table 1.

### 5.2. Filter paper measurements—engine 'A'

The DPF was removed (but with the DOC remaining) and the exhaust was drawn into the CVS tunnel. From the CVS tunnel (flow 6300 slpm on average) around 5 slpm on average was drawn through a filter paper holder and 8 slpm was drawn into the DMS500. Tunnel and filter flows were logged so that mass concentration in the tunnel could be calculated for both the filters and the DMS500. No further DMS primary dilution was used, although the secondary (rotating disc) diluter was used as necessary to bring the concentration within the dynamic range of the instrument. Two filters were taken back-to-back per test condition, with the DMS500 continuously logging. Table 2 summarises the test conditions and results.

### 5.3. Diesel particulate filter weighings—engine 'B'

A similar procedure was followed as for the DPF weighings on engine 'A' (Section 5.1). Torque, RPM and EGR level were varied to obtain a variety of test conditions. Engine speed and throttle position were set constant for each of these tests, whilst torque decreased over each test as the DPF was filled, due to increasing back-pressure. The average mass of soot on the DPF for this engine was 17 g. These data are summarised in Table 3.

Table 2  
Results from filter paper weighings on engine 'A'

Condition	Mean mass concentration/ $\mu\text{g cc}^{-1}$	
	Filter	DMS
15% load, 1500 rpm	$7.26 \times 10^{-3}$	$5.20 \times 10^{-3}$
	$7.08 \times 10^{-3}$	$4.71 \times 10^{-3}$
8% load, 2000 rpm	$3.51 \times 10^{-3}$	$2.47 \times 10^{-3}$
	$3.76 \times 10^{-3}$	$2.44 \times 10^{-3}$
15% load, 2000 rpm	$7.34 \times 10^{-3}$	$6.83 \times 10^{-3}$
	$6.91 \times 10^{-3}$	$6.68 \times 10^{-3}$
35% load, 1500 rpm	$7.03 \times 10^{-3}$	$5.18 \times 10^{-3}$
	$6.04 \times 10^{-3}$	$4.95 \times 10^{-3}$
8% load, 1500 rpm	$6.20 \times 10^{-3}$	$6.33 \times 10^{-3}$
	$7.05 \times 10^{-3}$	$7.40 \times 10^{-3}$
40% load, 1500 rpm	$9.29 \times 10^{-3}$	$6.67 \times 10^{-3}$
	$1.03 \times 10^{-2}$	$7.70 \times 10^{-3}$
Warmstart NEDC	$3.88 \times 10^{-3}$	$3.05 \times 10^{-3}$
	$4.10 \times 10^{-3}$	$3.37 \times 10^{-3}$

Table 3  
Results from DPF weighings on engine 'B'—mean values over each test

Engine RPM	EGR open (%)	Load/Nm	Mass concentration/ $\mu\text{g cc}^{-1}$	
			DPF	DMS
2053	58	24.1	0.190	0.175
2182	68	12.1	0.078	0.059
2172	55	26.6	0.228	0.200
2187	53	15.9	0.165	0.151
1801	53	31.3	0.171	0.153
2173	35	19.6	0.271	0.214
2236	43	24.5	0.139	0.110
2045	37	31.0	0.097	0.066

#### 5.4. Validation results

Fig. 16 shows the correlation between mass concentration as measured by the DMS500 and by the two gravimetric methods using both engines. The mean and standard deviation of the percentage difference of the DMS measurements from the gravimetric measurements are:  $-15.1 \pm 18.0\%$  for the filter paper on engine 'A',  $-2.0 \pm 12.2\%$  for the DPF data on engine 'A' and  $-17.1 \pm 6.8\%$  for the DPF data on engine 'B': overall it is  $-12.1 \pm 11.4\%$  for the DPF weighings. For all tests the difference is  $-13.7 \pm 15.3\%$ . In general the DMS reads the lower of the two. In the case of the filter papers, some of this is explained by the adsorption of volatiles onto the paper. Some may also be explained by the possible presence of a third,  $> 1\mu\text{m}$ , coarse mode in the tailpipe (reentrainment of PM from surfaces), which can contain up to 20% of the mass, but is negligible in terms of number concentration (Kittelson et al., 2002).

## 6. Conclusions

A new Bayesian statistical data processing algorithm for the DMS500 has been developed, which reduces the noise on mass calculation by a factor of nine and automatically discriminates between nucleation and accumulation modes. It also improves spectral resolution and provides a convenient means to summarise large data sets.

Differences in charging lead to agglomerates being differently sized by DMAs and DMS type instruments (with the latter calibrated for spherical aerosols)—these differences have been quantified for the DMS500 and whilst small for particles  $< 100\text{ nm}$ , will have some effect for larger particles and hence a significant effect for mass calculation. Taking

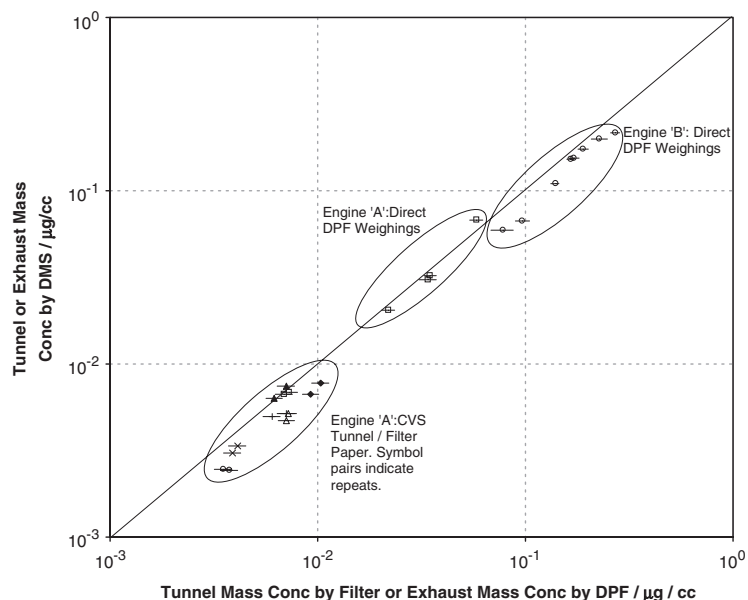


Fig. 16. Consolidated results of comparison between particulate mass concentration measured by DMS and gravimetric methods. Line indicates 1:1 correspondence and is not a line of best fit to the data. Errors in DPF weighings are based upon the precision of the balance used, those for filter measurements are based upon the mean 9.3% coefficient of variance for filter paper measurements given by Andersson and Dilara (2005). The error bars do not take into account adsorption or other artefacts.

this difference into account, data from other workers have been used to predict a size to mass power-law relationship for the DMS500, with an index of 3.19. The effective density as a function of size for the DMS was found to be closer in both magnitude and independence of size to those for water/sulphuric acid droplets than equivalent relationships for the DMA in the literature, therefore making DMS mass calculation less susceptible to error caused by these liquids being adsorbed on agglomerates.

Validation data for the mass calculation technique were taken on two different light duty common rail diesel engines and agreement with gravimetric methods was on average  $-13.7\%$ . Whilst subject to a small systematic underestimation, this is good given that the mass calculation is based upon fundamental calibrations and measurements independent of direct measurement of the validation aerosols considered, with the exception that one of the engines was used to determine the DMS:DMA size relationship. Given the systematic underestimation by the DMS, the application of empirical calibration (for example with the CPMA) would lead to more accurate results still.

Further work will include such CPMA based calibration, and obtaining more validation data on a wider variety of engines and fuel types including post-DPF sampling. On-road validation using the vehicle of engine 'A' and the DMS50 mobile particle sizer is also planned.

## References

- Ahlvik, P., Ntziachristos, L., Keskinen, J., & Virtanen, A., 1998. Real time measurements of diesel particle size distribution with an electrical low pressure impactor. *SAE Technical Paper*, 980410.
- Andersson, J., & Dilara, P. (2005). *UN-ECE particle measurement programme (PMP) light duty inter-laboratory correlation exercise, report on first results*. Technical Report, European Commission.
- Andrews, G. E., Clark, A. G., Rojas, N. Y., Sale, T., & Gregory, D. (2001). Diesel particle size distribution: The conversion of particle number size distribution to mass distribution. *SAE Technical Paper*, 2001-01-1946.
- Biskos, G., Reavell, K., & Collings, N. (2005). Unipolar diffusion charging of aerosol particles in the transition regime. *Journal of Aerosol Science*, 36, 247–265.
- Campbell, B., Peckham, M., Symonds, J., Parkinson, J., & Finch, A. (2006). Transient gaseous and particulate emissions measurements on a diesel passenger car including a DPF regeneration event. *SAE Technical Paper*, 2006-01-1079.
- Chan, S. H., & He, Y. S. (1999). Measurements of particulate mass concentration using a tapered-element oscillating microbalance and a flame ionization detector. *Measurement Science and Technology*, 10, 323–332.

- Ehara, K., Hagwood, C., & Coakley, K. J. (1996). Novel method to classify aerosol particles according to their mass-to-charge ratio—aerosol particle mass analyser. *Journal of Aerosol Science*, 27, 217–234.
- Gulijk, C. V., Marijnissen, J., Makkee, M., Moulijn, J., & Schmidt-Ott, A. (2004). Measuring diesel soot with a scanning mobility particle sizer and an electrical low-pressure impactor: performance assessment with a model for fractal-like agglomerates. *Journal of Aerosol Science*, 35, 633–655.
- Hinds, W. C. (1999). *Aerosol Technology*. (2nd ed.), New York: Wiley.
- Johnson, T., Caldow, R., Pocher, A., Mirme, A., & Kittelson, D. (2004). An engine exhaust particle sizer spectrometer for transient emission particle measurements. *SAE Technical Paper*, 2004-01-1341.
- Kasper, G. (1982). Dynamics and measurement of smokes. *Aerosol Science and Technology*, 1, 187–199.
- Kelly, W., & McMurry, P. (1992). Measurement of particle density by inertial classification of differential mobility analyzer-generated monodisperse aerosols. *Aerosol Science and Technology*, 17, 199–212.
- Khalek, I. A., Kittelson, D. B., & Brear, F. (2000). Nanoparticle growth during dilution and cooling of diesel exhaust: Experimental investigation and theoretical assessment. *SAE Technical Paper*, 2000-01-0515.
- Kittelson, D., Hands, T., Nickolaus, C., Collings, N., Niemelä, V., & Twigg, M. (2004). Mass correlation of engine emissions with spectral instruments. *JSAE Annual Congress Technical Paper*, 20045462.
- Kittelson, D., Watts, W., & Johnson, J. (2002). Diesel aerosol sampling methodology—CRC E-43: Final report. *Technical Report*, University of Minnesota Department of Mechanical Engineering.
- Lehmann, U., Niemelä, V., & Mohr, M. (2004). New method for time-resolved diesel engine exhaust particle mass measurement. *Environmental Science and Technology*, 38, 5704–5711.
- Mandelbrot, B. B. (1983). *The Fractal Geometry of Nature*. New York: W.H. Freeman and Company.
- Maricq, M. M., & Xu, N. (2004). The effective density and fractal dimension of soot particles from premixed flames and motor vehicle exhaust. *Journal of Aerosol Science*, 35, 1251–1274.
- Marple, V. A., Rubow, K. L., & Behm, S. M. (1991). A microorifice uniform deposit impactor (MOUDI): Description, calibration, and use. *Aerosol Science and Technology*, 14, 434–446.
- McMurry, P. H., Wang, X., Park, K., & Ehara, K. (2002). The relationship between mass and mobility for atmospheric particles: A new technique for measuring particle density. *Aerosol Science and Technology*, 36, 227–238.
- Mirme, A., Noppel, M., Piel, I., Salm, J., Tamm, E., & Tammet, H. (1984). Multi-channel electric aerosol spectrometer. In: *11th international conference on atmospheric aerosols, condensation and ice nuclei*. (pp. 155–159).
- Morawska, L., Johnson, G., Ristovski, Z. D., & Agranovski, V. (1999). Relation between particle mass and number for submicrometer airborne particles. *Atmospheric Environment*, 33, 1983–1990.
- Olfert, J., & Collings, N. (2005). New method for particle mass classification—The Couette centrifugal particle mass analyzer. *Journal of Aerosol Science*, 36, 1338–1352.
- Olfert, J. S., Symonds, J. P. R., & Collings, N. (2006). The effective density and fractal dimension of particles emitted from a light-duty diesel vehicle with a diesel oxidation catalyst. *Journal of Aerosol Science*, in press, doi:10.1016/j.jaerosci.2006.10.002.
- Park, K., Cao, F., Kittelson, D. B., & McMurry, P. H. (2003). Relationship between particle mass and mobility for diesel exhaust particles. *Environmental Science and Technology*, 37, 577–583.
- Patashnick, H., Rupprecht, G., Ambs, J. L., & Meyer, M. B. (2001). Development of a reference standard for particulate matter mass in ambient air. *Aerosol Science and Technology*, 34, 42–45.
- Peters, T. M., Chein, H., & Lundgren, D. A. (1993). Comparison and combination of aerosol size distributions measured with a low pressure impactor, differential mobility particle sizer, electrical aerosol analyzer, and aerodynamic particle sizer. *Aerosol Science and Technology*, 19, 396–405.
- Petzold, A., & Niessner, R. (1996). Photoacoustic soot sensor for in-situ black carbon monitoring. *Applied Physics B: Lasers and Optics*, 63, 191–197.
- Pich, J. (1964). Impaction of aerosol particles in the neighborhood of a circular hole. *Collection of Czechoslovak Chemical Communication*, 29, 2223–2227.
- Reavell, K. (2002). Fast response classification of fine aerosols with a differential mobility spectrometer. *Proceedings of Aerosol Society AGM*, 121–124.
- Reavell, K., Hands, T., & Collings, N. (2002). A fast response particulate spectrometer for combustion aerosols. *SAE Technical Paper*, 2002-01-2714.
- Saito, K., & Shinozaki, O. (1990). The measurement of diesel particulate emissions with a tapered element oscillating microbalance and an opacimeter. *SAE Technical Paper*, 900644.
- Sioutas, C., Abt, E., Wolfson, J. M., & Koutrakis, P. (1999). Evaluation of the measurement performance of the scanning mobility particle sizer and aerodynamic particle sizer. *Aerosol Science and Technology*, 30, 84–92.
- Sioutas, C., Kim, S., Chang, M., Terrell, L. L., & Gong, H., Jr. (2000). Field evaluation of a modified DataRAM MIE scattering monitor for real-time mass concentration measurements. *Atmospheric Environment*, 34, 4829–4838.
- Sivia, D. (1994). *Data analysis: A Bayesian tutorial*. Oxford: New York.
- Symonds, J., Collings, N., Reavell, K. S., Kittelson, D. (2004). Evaporation of volatile aerosols. In: *8th ETH conference on combustion generated nanoparticles*. (p. 40).
- Thomas, A., & Gebhart, J. (1994). Correlations between gravimetry and light scattering photometry for atmospheric aerosols. *Atmospheric Environment*, 28, 935–938.
- Wang, S. C., & Flagan, R. C. (1990). Scanning electrical mobility spectrometer. *Aerosol Science and Technology*, 13, 230–240.
- Zhang, X. Q., & McMurry, P. H. (1987). Theoretical analysis of evaporative losses from impactor and filter deposits. *Atmospheric Environment*, 21, 1779–1789.